J|A|C|S ARTICLES

Published on Web 11/06/2009

2D Networks of Rhombic-Shaped Fused Dehydrobenzo[12]annulenes: Structural Variations under Concentration Control

Kazukuni Tahara,[†] Satoshi Okuhata,[†] Jinne Adisoejoso,[‡] Shengbin Lei,[‡] Takumi Fujita,[†] Steven De Feyter,[‡,*] and Yoshito Tobe[†,*]

Division of Frontier Materials Science, Graduate School of Engineering Science, Osaka University, Toyonaka, Osaka 560-8531 Japan and Department of Chemistry, Division of Molecular and Nanomaterials, Laboratory of Photochemistry and Spectroscopy, and Institute of Nanoscale Physics and Chemistry, Katholieke Universiteit Leuven (KULeuven), Celestijnenlaan 200 F, B-3001 Leuven, Belgium

Received June 3, 2009; E-mail: Steven.DeFeyter@chem.kuleuven.be (S.D.F.); tobe@chem.es.osaka-u.ac.jp (Y.T.)

Abstract: A series of alkyl- and alkoxy-substituted rhombic-shaped bisDBA derivatives **1a**−**d**, **2a**, and **2b** were synthesized for the purpose of the formation of porous networks at the 1,2,4-trichlorobenzene (TCB)/graphite interface. Depending on the alkyl-chain length and the solute concentration, bisDBAs exhibit five network structures, three porous structures (porous A, B, and C), and two nonporous structures (nonporous D and E), which are attributed to their rhombic core shape and the position of the substituents. BisDBAs **1a** and **1b** with the shorter alkyl chains favorably form a porous structure, whereas bisDBAs **1c** and **1d** with the longer alkyl chains are prone to form nonporous structures. However, upon dilution, nonporous structures are typically transformed into porous ones, a trend that can be understood by the effect of surface coverage, molecular density, and intermolecular interactions on the system's enthalpy. Furthermore, porous structures are stabilized by the coadsorption of solvent molecules. The most intriguing porous structure, the Kagomé pattern, was formed for all compounds at least to some extent, and the size of its triangular and hexagonal pores could be tuned by the alkyl-chain length. The present study proves that the concentration control is a powerful and general tool for the construction of porous networks at the liquid−solid interface.

Introduction

Construction of 2D molecular networks on solid surfaces based on self-assembly[1] is a subject of intense interest owing to the perspective of various applications in the field of nanoscience and nanotechnology.[2] Supramolecular self-assembly can become an alternative for current lithographic techniques to create surface patterns in the low nanometer regime.[3] The design and control of the structure and functionality of molecular networks requires insight in the correlation between molecular structural features (shape, nature, and position of interacting sites) as well as molecular electronic properties and the topology of surface-confined molecular architectures. This strategy is known as crystal engineering and has rapidly developed in 2D systems.[1,4,5] Among various types of molecular networks, porous 2D molecular networks have received a lot of attention because such surface-confined molecular networks can accommodate

* To whom correspondence should be addressed.
† Osaka University.
‡ K.U. Leuven.

(1) (a) Frommer, J. *Angew. Chem., Int. Ed.* **1992**, *31*, 1298–1328. (b) Walba, D. M.; Stevens, F.; Clark, N. A.; Parks, D. *Acc. Chem. Res.* **1996**, *29*, 591–597. (c) Barth, J. V. *Annu. Rev. Phys. Chem.* **2007**, *58*, 375–407. (d) Theobald, J. A.; Oxtoby, N. S.; Phillips, M. A.; Champness, N. R.; Beton, P. H. *Nature* **2003**, *424*, 1029–1031. (e) Giancarlo, L. C.; Flynn, G. W. *Acc. Chem. Res.* **2000**, *33*, 491–501. (f) Samorì, P.; Rabe, J. P. *J. Phys.: Condens. Matter* **2002**, *14*, 9955–9973. (g) De Feyter, S.; De Schryver, F. C. *J. Phys. Chem. B* **2005**, *109*, 4290–4302. (h) Barth, J. V.; Costantini, G.; Kern, K. *Nature* **2005**, *437*, 671–679. (i) Wan, L.-J. *Acc. Chem. Res.* **2006**, *39*, 334–342. (j) Hermann, B. A.; Scherer, L. J.; Housecroft, C. E.; Constable, E. C. *Adv. Funct. Mater.* **2006**, *16*, 221–235. (k) Surin, M.; Samorì, P. *Small* **2007**, *3*, 190–194. (l) Plass, K. E.; Grzesiak, A. L.; Matzger, A. J. *Acc. Chem. Res.* **2007**, *40*, 287–293.
(2) (a) Joachim, C.; Gimzewski, J. K.; Aviram, A. *Nature* **2000**, *408*, 541–548. (b) Nitzan, A.; Ratner, M. A. *Science* **2003**, *300*, 1384–1389.
(3) Sheats, J. R.; Smith, B. W. *Microlithographic Science and Technology*, Marcel Dekker, 1st ed.; New York, 1998.
(4) (a) Schmidt, G. M. J. *Pure Appl. Chem.* **1971**, *27*, 647–678. (b) *Crystal Engineering: The Design of Organic Solid*; Desiraju, G. R.; Elsevier: New York, 1989. (c) Desiraju, G. R. *Angew. Chem., Int. Ed. Engl.* **1995**, *34*, 2311–2327. (d) Blagden, N.; Davey, R. J. *Cryst. Growth Des.* **2003**, *3*, 873–885.
(5) Furukawa, S.; De Feyter, S. *Top. Curr. Chem.* **2008**, *287*, 87–113.
(6) (a) Stepanow, S.; Lingenfelder, M.; Dmitriev, A.; Spillmann, H.; Delvigne, E.; Lin, N.; Deng, X.; Cai, C.; Barth, J. V.; Kern, K. *Nat. Mat.* **2004**, *3*, 229–233. (b) Lu, J.; Lei, S. B.; Zeng, Q. D.; Kang, S. Z.; Wang, C.; Wan, L. J.; Bai, C. L. *J. Phys. Chem. B* **2004**, *108*, 5161–5165. (c) Griessl, S. J. H.; Lackinger, M.; Jamitzky, F.; Markert, T.; Hietschold, M.; Heckl, W. M. *J. Phys. Chem. B* **2004**, *108*, 11556–11560. (d) Griessl, S. J. H.; Lackinger, M.; Jamitzky, F.; Markert, T.; Hietschold, M.; Heckl, W. M. *Langmuir* **2004**, *20*, 9403–9407. (e) Liu, Y.; Lei, S.; Yin, S.; Xu, S.; Zheng, Q.; Zeng, Q.; Wang, C.; Wan, L.; Bai, C. *J. Phys. Chem. B* **2002**, *106*, 12569–12574. (f) Schull, G.; Douillard, L.; Fiorini-Debuisschert, C.; Charra, F.; Mathevet, F.; Kreher, D.; Attias, A.-J. *Nano Lett.* **2006**, *6*, 1360–1363. (g) Kudernac, T.; Lei, S.; Elemans, J. A. A. W.; De Feyter, S. *Chem. Soc. Rev.* **2009**, *38*, 402–421.

guest molecules or atomic clusters via so-called 2D host−guest chemistry, resulting in the formation of multicomponent nanostructures.[6,7] These molecular networks are typically observed by means of scanning tunneling microscopy (STM) under ultrahigh vacuum (UHV) conditions or at the liquid−solid interface.[1]

The control of molecule−molecule interactions is crucial especially for the formation of such porous molecular networks: typically, discrete molecular building-blocks have to be connected to each other by virtue of directional intermolecular interactions such as hydrogen bonding,[8] dipolar coupling,[9] metal coordination,[10] or simply based upon van der Waals interactions between (interdigitating) alkyl chains.[11−14] In addition to molecule−molecule interactions, molecule−substrate interactions are also playing a key role in determining the network topologies. For example, it is well-documented that the molecular network structure can be affected by tuning molecule−graphite van der Waals interactions as a result of changing the length of linear alkanes[15,16] or alkyl chains of alkylated molecules.[17] More specifically, epitaxial stabilization by matching of 2D lattice registry between the molecular layer and the substrate layer is also important for the molecular arrangement.[18] Obviously, solvent plays an important role too at a liquid/solid interface. For instance, it affects the adsorption−desorption equilibrium,[19] and solvent molecules can even become part of the molecular network (so-called coadsorption).[20] In addition, solute concentration affects network formation especially for nanoporous systems, an aspect that has been revealed only recently. More specifically, in the case of alkoxylated triangular dehydrobenzo[12]annulene (DBA) derivatives, two patterns (nonporous linear and porous honeycomb structures) appear depending on the concentration; nonporous linear structures are formed at high solute concentrations, whereas porous honeycomb structures are favored upon dilution.[21] The relative abundance of both structures also depends on the alkoxy chain length. The tendency to form porous honeycomb structures decreases with increasing alkyl-chain length, which is supported by semiquantitative thermodynamics modeling. A second beautiful example of the concentration effect is the binary mixture of trimesic acid (TMA) and 1,3,5-tris(4-carboxylphenyl)benzene (BTB).[22] This mixture exhibits two polymorphs of TMA, one 2D pattern from BTB, and three patterns of cocrystals depending on the ratios of both components and their concentrations. A phase diagram of the six patterns was presented based on a thermodynamic equilibrium model. Moreover, the effect of solute concentration was also demonstrated for the formation of a porous molecular network from

(7) (a) Furukawa, S.; Tahara, K.; De Schryver, F. C.; Van der Auweraer, M.; Tobe, Y.; De Feyter, S. *Angew. Chem., Int. Ed.* **2007**, *46*, 2831–2834. (b) Lei, S.; Tahara, K.; Feng, X.; Furukawa, S.; De Schryver, F. C.; Müllen, K.; Tobe, Y.; De Feyter, S. *J. Am. Chem. Soc.* **2008**, *130*, 7119–7129. (c) Tahara, K.; Lei, S.; Mössinger, D.; Kozuma, H.; Inukai, K.; De Schryver, F. C.; Höger, S.; Tobe, Y.; De Feyer, S. *Chem. Commun.* **2008**, 3897–3899. (d) Tahara, K.; Lei, S.; Mamdouh, W.; Yamaguchi, Y.; Ichikawa, T.; Uji-i, H.; Sonoda, M.; Hirose, K.; De Schryver, F. C.; De Feyter, S.; Tobe, Y. *J. Am. Chem. Soc.* **2008**, *130*, 6666–6667.

(8) There are a number of reports about the formation of 2D molecular networks through hydrogen bonding as connectivity. See, for example: (a) Griessl, S.; Lackinger, M.; Edelwirth, M.; Hietschold, M.; Heckl, W. M. *Single Mol.* **2002**, *3*, 25–31. (b) Griessl, S. J. H.; Lackinger, M.; Jamitzky, F.; Markert, T.; Hietschold, M.; Heckl, W. M. *Langmuir* **2004**, *20*, 9403–9407. (c) Lei, S. B.; Wang, C.; Yin, S. X.; Wang, H. N.; Xi, F.; Liu, H. W.; Xu, B.; Wan, L. J.; Bai, C. L. *J. Phys. Chem. B* **2001**, *105*, 10838–10841. (d) Otsuki, J.; Nagamine, E.; Kondo, T.; Iwasaki, K.; Asakawa, M.; Miyake, K. *J. Am. Chem. Soc.* **2005**, *127*, 10400–10405. (e) Mamdouh, W.; Kelly, R. E. A.; Dong, M.; Kantorovich, L. N.; Besenbacher, F. *J. Am. Chem. Soc.* **2008**, *130*, 695–702.

(9) (a) Yokoyama, T.; Yokoyama, S.; Kamikado, T.; Okuno, Y.; Mashiko, S. *Nature* **2001**, *413*, 619–621. (b) de Wild, M.; Berner, S.; Suzuki, H.; Yanagi, H.; Schlettwein, D.; Ivan, S.; Baratoff, A.; Guentherodt, H. J.; Jung, T. A. *ChemPhysChem* **2002**, *3*, 881–885. (c) Wei, Y.; Tong, W.; Wise, C.; Wei, X.; Armbrust, K.; Zimmt, M. *J. Am. Chem. Soc.* **2006**, *128*, 13362–13363. (d) Wei, Y.; Tong, W.; Zimmt, M. B. *J. Am. Chem. Soc.* **2008**, *130*, 3399–3405.

(10) (a) Lingenfelder, M. A.; Spillmann, H.; Dmitriev, A.; Stepanow, S.; Lin, N.; Barth, J. V.; Kern, K. *Chem.—Eur. J.* **2004**, *10*, 1913–1919. (b) Stepanow, S.; Lin, N.; Payer, D.; Schilckum, U.; Klappenberger, F.; Zoppellaro, G.; Ruben, M.; Brune, H.; Barth, J. V.; Kern, K. *Angew. Chem., Int. Ed.* **2007**, *46*, 710–713. (c) Surin, M.; Samorì, P.; Jouaiti, A.; Kyritsakas, N.; Hosseini, M. W. *Angew. Chem., Int. Ed.* **2007**, *46*, 245–249.

(11) (a) Qiu, X.; Wang, C.; Zeng, Q.; Xu, B.; Yin, S.; Wang, H.; Xu, S.; Bai, C. *J. Am. Chem. Soc.* **2000**, *122*, 5550–5556. (b) Bléger, D.; Kreher, D.; Mathevet, F.; Attias, A.-J.; Schull, G.; Huard, A.; Douillard, L.; Fiorini-Debuischert, C.; Charra, F. *Angew. Chem., Int. Ed.* **2007**, *46*, 7404–7407. (c) Bléger, D.; Kreher, D.; Mathevet, F.; Attias, A.-J.; Arfaoui, I.; Metgé, G.; Douillard, L.; Fiorini-Debuisschert, C.; Charra, F. *Angew. Chem., Int. Ed.* **2008**, *47*, 8412–8415.

(12) (a) Furukawa, S.; Uji-i, H.; Tahara, K.; Ichikawa, T.; Sonoda, M.; De Schryver, F. C.; Tobe, Y.; De Feyter, S. *J. Am. Chem. Soc.* **2006**, *128*, 3502–3503. (b) Tahara, K.; Furukawa, S.; Uji-i, H.; Uchino, T.; Ichikawa, T.; Zhang, J.; Sonoda, M.; De Schryver, F. C.; De Feyter, S.; Tobe, Y. *J. Am. Chem. Soc.* **2006**, *128*, 16613–16625.

(13) (a) Foster, J. S.; Frommer, J. E. *Nature* **1988**, *333*, 542–545. (b) Spong, J. K.; Mizes, H. A.; LaComb Jr, L. J.; Dovek, M. M.; Frommer, J. E.; Foster, J. S. *Nature* **1989**, *338*, 137–139. (c) Mizutani, W.; Shigeno, M.; Sakakibara, Y.; Kajimura, K.; Ono, M.; Tanishima, S.; Ohno, K.; Toshima, N. *J. Vac. Sci. Technol., A* **1990**, *8*, 675–678.

(14) (a) Walba, D. M.; Stevens, F.; Parks, D. C.; Clark, N. A.; Wand, M. D. *Science* **1995**, *267*, 1144–1147. (b) Parks, D. C.; Clark, N. A.; Walba, D. M.; Beale, P. D. *Phys. Rev. Lett.* **1993**, *70*, 607–610.

(15) (a) Smith, D. P. E.; Hörber, H.; Gerber, C.; Binning, G. *Science* **1989**, *245*, 43–45. (b) Smith, D. P. E.; Hörber, J. K. H.; Binning, G.; Nejoh, H. *Nature* **1990**, *344*, 641–644. (c) Hara, M.; Iwakabe, Y.; Tochigi, K.; Sasabe, H.; Garito, A. F.; Yamada, A. *Nature* **1990**, *344*, 228–230.

(16) (a) Paserba, K. R.; Gellman, A. J. *J. Chem. Phys.* **2001**, *115*, 6737–6751. (b) Paserba, K. R.; Gellman, A. J. *Phys. Rev. Lett.* **2001**, *86*, 4338–4341. (c) Müller, T.; Flynn, G. W.; Mathauser, A. T.; Teplyakov, A. V. *Langmuir* **2003**, *19*, 2812–2821.

(17) (a) Wu, P.; Zeng, Q.; Xu, S.; Wang, C.; Yin, S.; Bai, C. L. *ChemPhysChem* **2001**, *2*, 750–754. (b) Charra, F.; Cousty, J. *Phys. Rev. Lett.* **1998**, *80*, 1682–1685. (c) Askadskaya, L.; Boeffel, C.; Rabe, J. P. *Bunsenges. Phys. Chem.* **1993**, *97*, 517–521. (d) Ito, S.; Wehmeier, M.; Brand, J. D.; Kübel, C.; Epsch, R.; Rabe, J. P.; Müllen, K. *Chem.—Eur. J.* **2000**, *6*, 4327–4342. (e) Mena-Osteriz, E. *Adv. Mater.* **2002**, *14*, 609–616.

(18) (a) Hiller, A. C.; Ward, M. D. *Phys. Rev. B* **1996**, *54*, 14037–14051. (b) Hooks, D. E.; Fritz, T.; Ward, M. D. *Adv. Mater.* **2001**, *13*, 227–241.

(19) (a) Venkataraman, B.; Breen, J. J.; Flynn, G. W. *J. Phys. Chem.* **1995**, *99*, 6608–6619. (b) Li, C.-J.; Zeng, Q.-D.; Wang, C.; Wan, L.-J.; Xu, S.-L.; Wang, C.-R.; Bai, C.-L. *J. Phys. Chem. B* **2003**, *107*, 747–750. (c) Lackinger, M.; Griessl, S.; Heckl, W. M.; Hietschold, M.; Flynn, G. W. *Langmuir* **2005**, *21*, 4984–4988. (d) Kampschulte, L.; Lackinger, M.; Maier, A.-K.; Kishore, R. S. K.; Griessl, S.; Schmittel, M.; Heckl, W. M. *J. Phys. Chem. B* **2006**, *110*, 10829–10836. (e) Shao, X.; Luo, X.; Hu, X.; Wu, K. *J. Phys. Chem. B* **2006**, *110*, 1288–1293. (f) Gutzler, R.; Lappe, S.; Mahata, K.; Schmittel, M.; Heckl, W. M.; Lackinger, M. *Chem. Commun.* **2009**, 680–682.

(20) (a) Mamdouh, W.; Uji-i, H.; Ladislaw, J. S.; Dulcey, A. E.; Percec, V.; De Schryver, F. C.; De Feyter, S. *J. Am. Chem. Soc.* **2006**, *128*, 317–325. (b) Nath, K. G.; Ivasenko, O.; Miwa, J. A.; Dang, H.; Wuest, J. D.; Nanci, A.; Perepichka, D. F.; Rosei, F. *J. Am. Chem. Soc.* **2006**, *128*, 4212–4213. (c) Tahara, K.; Johnson, C. A., II; Fujita, T.; Sonoda, M.; De Schryver, F. C.; De Feyter, S.; Haley, M. M.; Tobe, Y. *Langmuir* **2007**, *23*, 10190–10197.

(21) Lei, S.; Tahara, K.; De Schryver, F. C.; Van der Auweraer, M.; Tobe, Y.; De Feyter, S. *Angew. Chem., Int. Ed.* **2008**, *47*, 2964–2968.

(22) Kampschulte, L.; Werblowsky, T. L.; Kishore, R. S. K.; Schmittel, M.; Heckl, W. M.; Lackinger, M. *J. Am. Chem. Soc.* **2008**, *130*, 8502–8507.

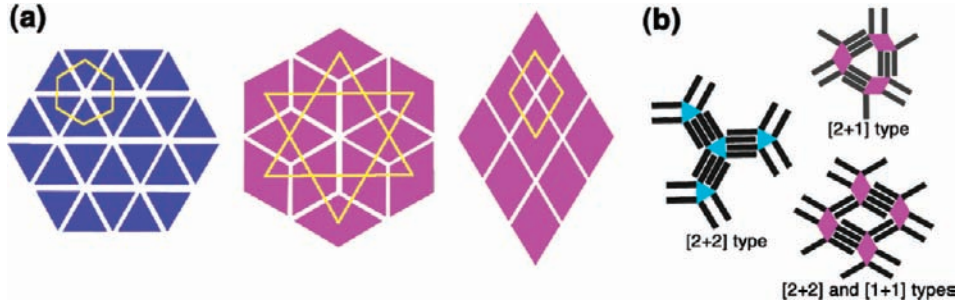

Figure 1. (a) Schematic view of dense packings of triangles and rhombi. (b) Three different types of alkyl-chain interdigitation: [2 + 2] (triangular DBAs) and [2 + 1] as well as a combination of [2 + 2] and [1 + 1] (rhombic bisDBAs). The yellow lines connecting the center of tiles highlight the different packing patterns.

melamine and linear bis-uracyl as well as diimide derivatives.[23] A threshold value of the hydrogen bond energy for the formation of the porous network was estimated. Hence, for a successful and rational construction of 2D molecular networks, tuning the different interaction modes discussed above as well as the solute concentration is essential.[24]

Among the various molecular networks, the porous Kagomé structure is particularly intriguing, not only because of the combination of both regularly arranged triangular and hexagonal pores in the network into which different guest molecule(s) or molecular cluster(s) can be entrapped forming multicomponents self-assembly patterns but also because of its relevance in the field of spin-frustrated magnetic materials.[25] Decyl-substituted rhombic-shaped bis(dehydrobenzo[12]annulene) (**1a**, bisDBA, Chart 1),[12] tetracarboxy-substituted *p*-bis(phenylethynyl)-benzene[26] and azobenzene,[27] and tetracyanoquinquephenyl[28] have been shown to form 2D molecular Kagomé networks. The apparently very different molecular building blocks share one common feature; they possess four sites (i.e., four nodes) dominating the directional intermolecular interactions via alkyl-chain interdigitations (van der Waals interactions) in the case of **1a** and via hydrogen bonding of four carboxy or cyano groups for the other three examples mentioned. More recently, the construction of Kagomé-type metal-organic frameworks involving Au atoms and (hexapyridyl)porphirin has also been demonstrated.[29] Additionally, a template (coronene)-induced formation of a Kagomé network has been achieved for a tetracarboxy-substituted *p*-quaterphenyl at a liquid−solid interface. In the absence of the template molecule, which is hosted in the hexagonal pores of the network, another polymorph is formed.[30] Despite this remarkable progress, size and functionality tuning of Kagomé networks is not achieved yet, and the anticipated particular host−guest chemistry of Kagomé networks − a network containing two types of pores − has only recently been explored.[31]

Chart 1. Molecular Structures of Rhombic-Shaped BisDBAs **1a**−**d**, **2a**, and **2b**

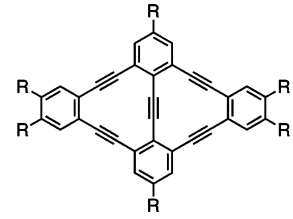

1a: R = $C_{10}H_{21}$
1b: R = $C_{12}H_{25}$
1c: R = $C_{14}H_{29}$
1d: R = $C_{16}H_{33}$
2a: R = $OC_{10}H_{21}$
2b: R = OC_9H_{19}

The following characteristics of the rhombic-shaped bisDBAs should be mentioned. First, there are two dense periodic rhombus tilings in two dimensions possible (part a of Figure 1, middle and right), one corresponding a Kagomé type pattern (part a of Figure 1, middle), whereas there is only one for triangles (part a of Figure 1, left) because of the lower symmetry of the rhombus. Note that aperiodic rhombus tilings exist, as recently demonstrated for a hydrogen bonded supramolecular system.[32] However, in case of the hexa-substituted bisDBAs, the molecules do not preserve the D_{2h} symmetry of the intrinsic rhombus, which is a requisite for the rhombus tiling shown in part a of Figure 1. Second, there are different motifs regarding the alkyl-chain interactions. The six peripheral substituents of the triangular DBAs lead to a [2 + 2]-type alkyl-chain interdigitation at all triangular sides (two alkyl chains per triangular side). In contrast, not all sides of the rhombus can be bridged via [2 + 2]-type interactions as there are only six alkyl chains for four nodes. The rhombus-shaped bisDBA system is expected to form two different motifs of interdigitating alkyl chains: a [2 + 1] type at all sides or a combination of [2 + 2]

(23) (a) Palma, C.-A.; Bonini, M.; Llanes-Pallas, A.; Breiner, T.; Prato, M.; Bonifazi, D.; Samorì, P. *Chem. Commun.* **2008**, 5289–5291. (b) Palma, C.-A.; Bjork, J.; Bonini, M.; Dyer, M. S.; Llanes-Pallas, A.; Bonifazi, D.; Persson, D.; Persson, M.; Samorì, P. *J. Am. Chem. Soc.* **2009**, *131*, 13062–13071.
(24) Palma, C.-A.; Bonini, M.; Breiner, T.; Samorì, P. *Adv. Mater.* **2009**, *21*, 1383–1386.
(25) (a) Syôzi, I. *Prog. Theor. Phys.* **1951**, *6*, 306–308. (b) Monauskis, E. *Rev. Mod. Phys.* **1991**, *63*, 1–62. (c) Nocera, D. G.; Bartlett, B. M.; Grohol, D.; Papoutsakis, D.; Shores, M. P. *Chem.—Eur. J.* **2004**, *10*, 3850–3859. (d) Rao, C. N. R.; Sampathkumaran, E. V.; Nagarajan, R.; Paul, G.; Behera, J. N.; Choudhury, A. *Chem. Mater.* **2004**, *16*, 1441–1446. (e) Pati, S. K.; Rao, N. R. *Chem. Commun.* **2008**, 4683–4693.
(26) Zhou, H.; Dang, H.; Yi, J.-H.; Nanci, A.; Rochefort, A.; Wuest, J. D. *J. Am. Chem. Soc.* **2007**, *129*, 13774–13775.
(27) Li, M.; Deng, K.; Lei, S.-B.; Yang, Y.-L.; Wang, T.-S.; Shen, Y.-T.; Wang, C.-R.; Zeng, Q.-D.; Wang, C. *Angew. Chem., Int. Ed.* **2008**, *47*, 6717–6721.
(28) Schlickum, U.; Decker, R.; Klappenberger, F.; Zoppellaro, G.; Klyatskaya, S.; Auwärter, W.; Neppl, S.; Kern, K.; Brune, H.; Ruben, M.; Barth, J. V. *J. Am. Chem. Soc.* **2008**, *130*, 11778–11782.
(29) Shi, Z.; Lin, N. *J. Am. Chem. Soc.* **2009**, *131*, 5376–5377.
(30) Blunt, M.; Lin, X.; Gimenez-Lopez, M.; del, C.; Schröder, M.; Champness, N. R.; Beton, P. H. *Chem. Commun.* **2008**, 2304–2306.
(31) Adisoejoso, J.; Tahara, K.; Okuhata, S.; Lei, S.; Tobe, Y.; De Feyter, S. *Angew. Chem., Int. Ed.* **2009**, *48*, 7353–7357.
(32) Blunt, M. O.; Russell, J. C.; Giménez-López, M.; del, C.; Garrahan, J. P.; Lin, X.; Schröder, M.; Champness, N. R.; Beton, P. H. *Science* **2008**, *322*, 1077–1081.

Scheme 1. Syntheses of BisDBA Derivatives **1a**−**d**, **2a**, and **2b**

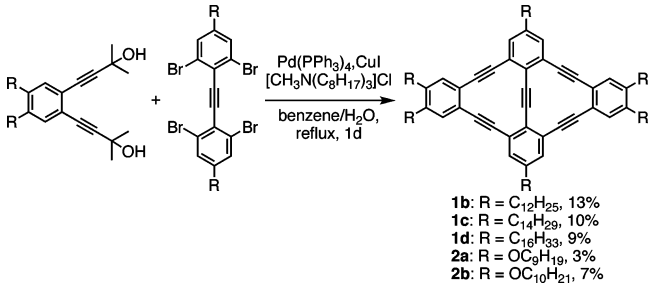

and [1 + 1] types (part b of Figure 1). Another characteristic of the 2D networks of the rhombic-shaped bisDBAs is their 2D chirality (Supporting Information for detail).

Gaining insight into the parameters controlling the outcome of supramolecular self-assembly on surfaces requires a systematic approach. The bisDBA system is in particular an intriguing case to be explored because of the possible control over the anticipated pattern variety. Therefore, the supramolecular network formation of alkylated or alkoxylated bisDBAs **1a**−**d**, **2a**, and **2b** at a liquid−solid interface has been investigated systematically using STM, highlighting the effect and role of the alkyl-chain length, and concentration dependency. In total, five structures are observed, three porous (porous A, porous B, and porous C) and two nonporous networks (nonporous D and nonporous E). These phenomena are discussed in terms of molecule−molecule, molecule−substrate, molecule−solvent, and solvent−substrate interactions and lead to a practical guide for the formation of porous (Kagomé) networks and their size control, specifically, and tuning the architecture of supramolecular networks composed from alkylated molecules in general.

Results and Discussion

1. Synthesis. The synthesis of bisDBA **1a** having six decyl chains (R = $C_{10}H_{21}$) was reported previously.[33] Following the previous procedure, we synthesized alkylated or alkoxylated bisDBAs **1b**−**d** and **2a**−**b** (R = $C_{12}H_{25}$; **1b**, $C_{14}H_{29}$; **1c**, $C_{16}H_{33}$; **1d**, $OC_{10}H_{21}$; **2a**, OC_9H_{19}; **2b**) from diethynylbenzene derivatives and tetrabromotolanes by the in situ deprotection Pd(0) catalyzed coupling protocol (Scheme 1). Details are described in the Supporting Information.

2. Self-Assembly of BisDBAs at the 1,2,4-Trichlorobenzene (TCB)/Graphite Interface. 2.1. Five Structures Formed by BisDBA Derivatives. All STM observations were performed at a 1,2,4-trichlorobenzene (TCB)/graphite interface at 19−24 °C. To allow stabilization of the system, all images were recorded by starting 1 to 2 h after bringing a drop of the TCB solution of bisDBAs **1a**−**d**, **2a**, and **2b** on top of the graphite substrate. The monolayer formation of bisDBAs was investigated at the interface at various solute concentrations (from 10^{-4} to 10^{-6} M) to evaluate the effect of different types of substituents (alkoxy or alkyl), the length of the alkyl chains, and the solute concentration on the geometry of the 2D networks. Figure 2 summarizes the five observed structures, the tentative molecular models constructed by molecular mechanics (MM) simulations with the MM3 parameters, and unit cells, ranked by increasing network density ($d_{structure}$, vide infra for the definition).

2.2. Porous Structures. First, we present the features of the three porous structures (porous A, B, and C). The porous A

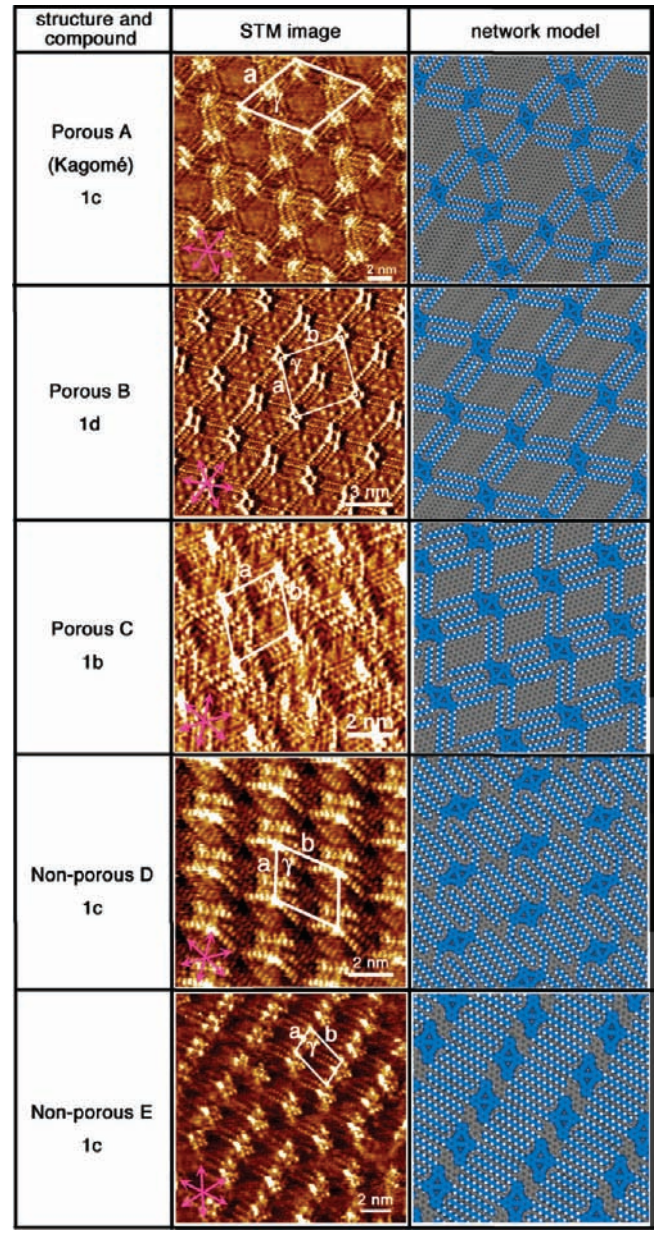

Figure 2. Overview of the five structures formed by the bisDBA derivatives: porous A (Kagomé), porous B, porous C, nonporous D, and nonporous E. The main symmetry directions of graphite ⟨1, −2, 1, 0⟩ are indicated in pink in the STM images (central column). Tentative network models (right column) are the result of molecular mechanics simulations with MM3 parameters using the experimental unit cell parameters as a periodic boundary condition (Supporting Information). In the model of the nonporous E structure, two alkyl chains per molecule orienting to the solution phase are omitted for clarity (I_{scl} = 0.09 nA, V_{bias} = −0.20 V for the porous A, I_{scl} = 0.40 nA, V_{bias} = −1.30 V for the porous B, I_{scl} = 0.45 nA, V_{bias} = −0.08 V for the porous C, I_{scl} = 0.06 nA, V_{bias} = −0.30 V for the nonporous D, and I_{scl} = 0.45 nA, V_{bias} = −0.25 V for the nonporous E).

structure corresponds to a Kagomé pattern (Figure 2, top row). As shown in the tentative model, all of the alkyl chains are adsorbed on the surface (the number of adsorbed alkyl chains: m = 6), aligning parallel to one of graphite's symmetry axes (the ⟨1, −2, 1, 0⟩ directions). Each π-core is bridged via a [2 + 1]-type alkyl-chain interdigitation. The bisDBA cores adopt three different orientations. The Kagomé structure contains two different types of pores, triangular and hexagonal ones.

In the porous B structure (Figure 2, second row), extended alkyl chains bridge the gap between adjacent DBA cores; this

(33) Sonoda, M.; Sakai, Y.; Yoshimura, T.; Tobe, Y.; Kamada, K. *Chem. Lett.* **2004**, 972–973.

leads to all [2 + 1]-type alkyl-chain interdigitation interactions between adjacent molecules. All alkyl chains align along two of the main symmetry axes of graphite ($m = 6$). The porous B structure has a rectangular pore.[34] In addition, whereas all molecules of the porous A structure are adsorbed with the same enantiotopic face within a given domain (conglomerate formation),[35] this is not the case for the porous B pattern (racemate formation, Supporting Information).

The porous C structure resembles the porous B structure as far as the number of adsorbed alkyl chains ($m = 6$) and the formation of rectangular pores are concerned (Figure 2, third row).[34] However, both structures can be clearly distinguished by comparison of the alignment of the alkyl chains in both patterns. For both patterns, all adsorbed alkyl chains run parallel to one of the main symmetry axes of graphite. However, the porous C pattern is characterized by twice [2 + 2] and twice [1 + 1] alkyl-chain interdigitation interactions,[36] whereas for the porous B-type alignment, alkyl-chain interdigitation interactions between adjacent molecules are all [2 + 1] type.

2.3. Nonporous Structures. Next, we discuss the structural aspects of the two densely packed nonporous structures, nonporous D and E. Similar to the porous B and C structures, the π-conjugated cores are oriented identically throughout a domain. In the nonporous D structure (Figure 2, fourth row), all alkyl chains are adsorbed ($m = 6$) along one of the graphite symmetric axes. Two of them most likely have gauche kinks to achieve favorable intermolecular van der Waals interactions.

On the other hand, in the nonporous E structure four alkyl chains per molecule are adsorbed ($m = 4$) with their axis parallel to a main symmetry axis of the graphite surface (Figure 2, bottom row). The other two alkyl chains are most likely to be exposed to the solution phase; each molecule is connected via two [2 + 2]-type alkyl-chain interdigitation interactions.

2.4. Concentration and Substituent Effects. The network coverage ($\theta_{network}$) of each structure was calculated by analyzing more than 10 large-area images (ca. 100 nm × 100 nm) for each compound at different concentrations. The concentration-dependent evolution of the network coverage of bisDBAs **1b**, **1c**, and **1d** is summarized in Figure 3 and in Tables S1−S3 of the Supporting Information. Details of the unit cell parameters for all observed structures of all compounds are provided in Table 1. The network density ($d_{structure}$) was estimated by dividing the unit cell area (*area*) by the number of molecules in the unit cell (Z). For a molecule with a given alkyl-chain length, the order of the network density ($d_{structure}$) of each structure is as follows: porous A ≤ porous B < porous C < nonporous D ≤ nonporous E (Figure 4).

BisDBA **1a** exclusively forms the porous A (Kagomé) structure for a wide concentration range (from 10^{-4} to 10^{-6} M).[12] In contrast, the bisDBA analogues with longer alkyl chains form a variety of concentration-dependent structural variations.

With two extra methylene groups in the alkyl chain, bisDBA **1b** forms the porous C structure (the third row in Figure 2) at a solute concentration of 7.0×10^{-4} M. Upon decreasing the solute concentration, the porous C structure is gradually replaced by the porous A (Kagomé) structure (Figure S6 of the Supporting Information). The concentration-dependent change of the surface coverage of each pattern is summarized in part a of Figure 3. The Kagomé structure appears at a solute concentration of 4.0×10^{-6} M, and its surface coverage (θ_A) reaches 30% at the lowest concentration probed (1.5×10^{-6} M).

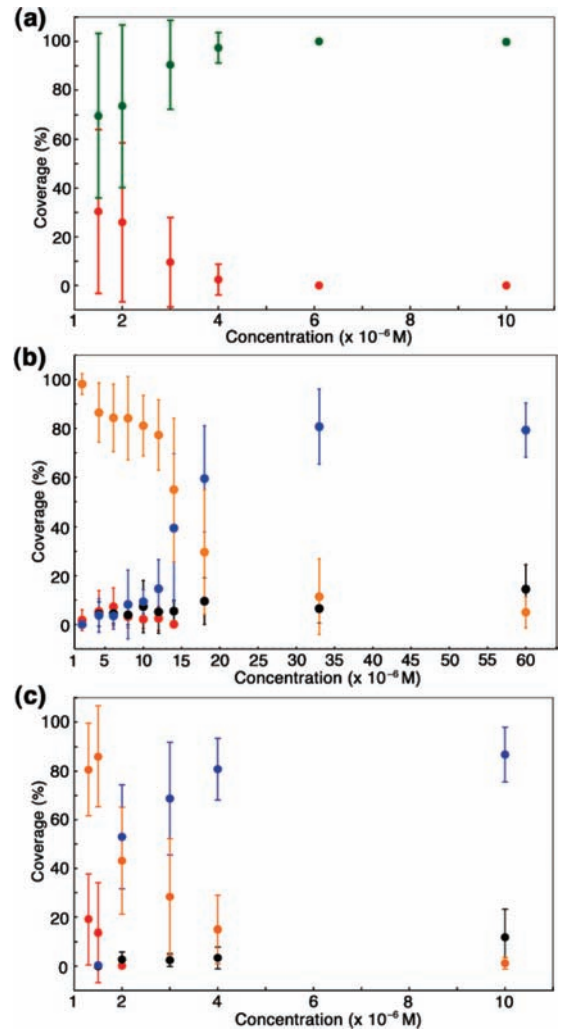

Figure 3. Concentration-dependent surface coverage of the five structures, porous A (θ_A, red), porous B (θ_B, orange), porous C (θ_C, green), nonporous D (θ_D, blue), and nonporous E (θ_E, black), of bisDBAs **1b** (a), **1c** (b), and **1d** (c) at the TCB−graphite interface.

The concentration-dependent surface coverage of the polymorphs of **1c** is summarized in part b of Figure 3. A remarkable change appears for this molecule. The relative surface coverage of the two nonporous linear structures (nonporous D and E, the fourth and bottom rows in Figure 2, respectively) does not change at concentrations higher than 3.3×10^{-5} M. Upon decreasing the solute concentration, the porous B structure (Figure S7 of the Supporting Information) rapidly becomes the dominant one ($\theta_B = 81\%$ at 1.0×10^{-5} M) with decreasing coverage of the nonporous patterns. The porous C structure only appears at domain boundaries ($\theta_C < 1\%$, Figure S8 of the Supporting Information). The porous A structure appears upon decreasing the concentration: its coverage reaches a maximum ($\theta_A = 7\%$) at 6.1×10^{-6} M (the top row in Figure 2). However, upon further decreasing the concentration down to 2.0×10^{-6} M the Kagomé structure disappears.

(34) Recently, Matzger et al. reported the formation of 2D rhomnic pores by alkoxyformamide in which alkyl groups are interdigitated in a [2 + 1] form. Ahn, S.; Morrison, C. N.; Matzger, A. J. *J. Am. Chem. Soc.* **2009**, *131*, 7946–7947.

(35) Eliel, E. L.; Wilen, S. H. *Stereochmistry of Organic Compounds*; Jon Wiley & Sons: New York, 1998; p 159.

(36) The porous B structure was observed for bisDBA **1a** as the kinetic phase within 10 min after sample preparation. See also ref 12b in which it is referred to as the linear A structure. For bisDBA **1b**, it appears as the stable phase under our experimental conditions.

Table 1. Structural Parameters of Monolayer Structure of BisDBAs **1a**−**d**, **2a**, and **2b**

			Unit Cell Parameters[a]								
compound	structure	plane group	*a* (nm)	*b* (nm)	γ (°)	*Z*[b]	*area* (nm^2)[c]	*D* (nm^{-2})[d,e]	*pore area* (nm^2)[f]	azimuthal angles (°)[g]	*m*[h]
1a	porous A (Kagomé)	*P6*	4.9 ± 0.1	4.9 ± 0.1	60 ± 1	3	21.2	0.141 (11.9)	8.3 (0.39)	15 ± 1	6
1b	porous A (Kagomé)	*P6*	5.4 ± 0.1	5.4 ± 0.1	61 ± 2	3	25.5	0.118 (11.3)	10.5 (0.41)	14 ± 1	6
	porous C	*P1*	2.7 ± 0.1	2.8 ± 0.2	78 ± 2	1	7.4	0.135 (13.0)	2.4 (0.32)	7 ± 1, 21 ± 3	6
1c	porous A (Kagomé)	*P6*	5.9 ± 0.1	5.9 ± 0.1	59 ± 1	3	29.8	0.101 (10.9)	12.8 (0.43)	12 ± 1	6
	porous B	*P2gg*	4.4 ± 0.1	4.4 ± 0.1	89 ± 1	2	19.4	0.103 (11.2)	8.0 (0.41)	0 ± 1, 29 ± 1	6
	nonporous D	*P1*	3.0 ± 0.1	3.1 ± 0.1	48 ± 1	1	6.9	0.145 (15.6)	--	7 ± 3, 19 ± 3	6
	nonporous E	*P1*	1.8 ± 0.1	3.0 ± 0.1	70 ± 2	1	5.1	0.197 (15.8)	--	24 ± 1, 19 ± 2	4
1d	porous A (Kagomé)	*P6*	6.4 ± 0.3	6.4 ± 0.3	60 ± 1	1	35.5	0.085 (10.2)	16.7 (0.47)	13 ± 2	6
	porous B	*P2gg*	4.7 ± 0.1	4.8 ± 0.1	88 ± 1	2	22.6	0.089 (10.6)	10.0 (0.44)	0 ± 1, 30 ± 1	6
	nonporous D	*P1*	3.0 ± 0.1	3.2 ± 0.1	51 ± 1	1	7.5	0.134 (16.1)	--	8 ± 1, 21 ± 2	6
	nonporous E	--[i]	--	--	--	-	--	--	--	--	--
2a	porous C	*P1*	2.5 ± 0.1	2.7 ± 0.1	77 ± 2	1	6.6	0.152 (13.7)	2.0 (0.30)	3 ± 2, 15 ± 4	6
2b	porous C	*P1*	2.4 ± 0.1	2.5 ± 0.1	78 ± 2	1	5.8	0.170 (14.3)	1.6 (0.28)	6 ± 1, 26 ± 1	6

[a] Unit cells are shown in the respective STM images. [b] Number of molecules per unit cell. [c] Unit cell area. [d] Network density (molecule/nm^2). [e] (number of adsorbed carbon atoms)/(area per unit cell) is given in parentheses. [f] The fraction of pore area (ρ) is given in parentheses. [g] Experimentally determined azimutal angles between the underling graphite unit cell vector and unit cell vector *a* (left) or *b* (right) of the molecular network. [h] Number of the adsorbed alkyl chains per bisDBA molecule. [i] Because of the lack of long-range order (Figure S10 of the Supporting Information), the unit cell parameters were not determined.

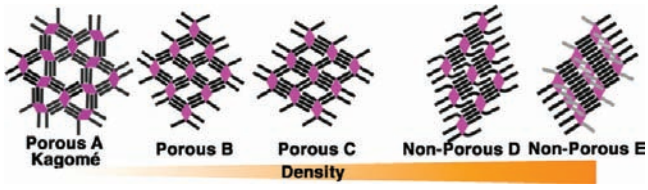

Figure 4. Summary of the observed molecular networks of bisDBAs and their relative molecular density.

In case of bisDBA **1d**, again, the relative surface coverage of the two nonporous structures (nonporous D and E, Figures S9 and S10 of the Supporting Information) does not change anymore at concentrations higher than 1.0×10^{-5} M (part c of Figure 3). Upon decreasing the solute concentration ($< 4.0 \times 10^{-6}$ M), the porous B structure (Figure 2, the second row) becomes the predominant structure ($\theta_B = 86\%$ at 1.5×10^{-6} M), a process that goes along with a drastic decrease of the surface coverage of the nonporous D structure. At concentrations below 2×10^{-6} M, the coverage of the Kagomé structure gradually increases reaching a maximum at the lowest concentration probed ($\theta_A = 19\%$, 1.3×10^{-6} M, Figure S11 of the Supporting Information). Here we observe a remarkable transition of the chirality characteristics of the physisorbed patterns as a function of surface coverage. For the high-density nonporous structures, all molecules within a given 2D domain have the same enantiotopic face directed to the surface and a homochiral lattice is formed. Obviously, other domains show the mirror-image-type pattern leading to a conglomerate. In contrast, in the lower-density porous B phase, a domain exists of a heterochiral lattice of molecules leading to a racemic compound.[37] The lowest-density pattern, the porous A or Kagomé pattern, forms again a homochiral phase at the level of a domain though. These observations[38] are intriguing in relation to the Wallach's rule[39] established in the 3D system, which states that a racemic lattice packs more densely than a homochiral lattice.

Contrary to the alkyl-substituted bisDBAs **1a**−**d**, bisDBAs **2a** and **2b** with alkoxy substituents only form the porous C structure at the wide concentration range probed (from 10^{-4} to 10^{-6} M). Details are described in Figures S12 and S13 of the Supporting Information. This is probably because of the different orientation of the alkoxy chains originating from the ether functionality.

Two general trends are elucidated from the above results: 1) at the level of the *solute concentration*: the lower the concentration, the larger the chance to find a low density pattern, and 2) at the level of the *alkyl-chain length*: the shorter the alkyl chains of the bisDBA derivatives, the stronger the tendency to form porous networks.[40]

These results are in line with the experimental trends observed for a related alkylated, triangular-shaped DBA system, which gives rise to only two patterns, a porous (honeycomb) and a nonporous (linear) one.[21,41] A similar concentration−monolayer density dependency has also been experimentally verified and theoretically confirmed for an alkyl-chain free bicomponent

(37) There are few reports on the network consisting of racemates from both chiral (racemic) and prochiral molecules. (a) De Feyter, S.; Gesquière, A.; Wurst, K.; Amabilino, D. B.; Veciana, J.; De Schryver, F. C. *Angew. Chem., Int. Ed.* **2001**, *40*, 3217–3220. (b) Hibino, M.; Sumi, A.; Tsuchiya, H.; Hatta, I. *J. Phys. Chem. B* **1998**, *102*, 4544–4547. (c) Wei, Y.; Kannappan, K.; Flynn, G. W.; Zimmt, M. B. *J. Am. Chem. Soc.* **2004**, *126*, 5318–5322.

(38) There are a number of reports on the formation of homochiral lattice on the surface from chiral as well as prochiral molecules. See, for example: (a) Stevens, F.; Dyer, D. J.; Walba, D. M. *Angew. Chem., Int. Ed.* **1996**, *35*, 900–901. (b) Cortés, R.; Mascaraque, A.; Schmidt-Weber, P.; Dil, H.; Kampen, T. U.; Horn, K. *Nano Lett.* **2008**, *8*, 4162–4167. (c) Vidal, F.; Delvigne, E.; Stepanow, S.; Lin, N.; Barth, J. V.; Kern, K. *J. Am. Chem. Soc.* **2005**, *127*, 10101–10106. (d) Rankin, R. B.; Sholl, D. S. *J. Phys. Chem. B* **2005**, *109*, 16764–16773. (e) Böhringer, M.; Schneider, W.-D.; Berndt, R. *Angew. Chem., Int. Ed.* **2000**, *39*, 792–795. (f) Huang, T.; Hu, Z.; Zhao, A.; Wang, H.; Wang, B.; Yang, J.; Hou, J. G. *J. Am. Chem. Soc.* **2007**, *129*, 3857–3862. (g) Fasel, R.; Parschau, M.; Ernst, K.-H. *Nature* **2006**, *439*, 449–452.

(39) Wallach, O. *Liebigs Ann. Chem.* **1895**, *286*, 90–143.

(40) Similar alkyl-chain length dependency was observed in the formation of porous versus nonporous 2D molecular networks of alkoxyformamides: See, ref 34.

(41) In our attempt to apply a thermodynamic model to evaluate the concentration-dependent polymorph appearance of the bisDBAs; however, we were confronted with difficulties: for example, in the case of **1b**, the high sensitivity of the network coverage to the solute concentration (i.e. rapid morphology change within a narrow concentration range) together with the large errors in the surface coverage hamper application of the quantitative treatment (Supporting Information). Furthermore, in the cases of **1c** and **1d**, the situation is more complicated because of the coexistence of more than two polymorphs.

(42) The details of the molecular mechanics simulations (MM3) are described in the Supporting Information.

(43) EpiCalc was downloaded on the Ward's group web site (http://www.nyu.edu/fas/dept/chemistry/wardgroup/Software.html).

Table 2. Representative Parameters for Geometric Epitaxy Calculated by the *EpiCalc* Program[a]

		Calculated Unit Cell Parameters				
compound	structure	b_1 (nm)	b_2 (nm)	β (°)	θ_{calcd}	V/V_0[b]
1a	porous A (Kagomé)	4.860	4.865	59.2	15.25	0.50
1b	porous A (Kagomé)	5.400	5.460	61.1	14.75	0.51
	porous C	2.645	2.820	77.1	23.75	0.50
1c	porous A (Kagomé)	5.905	5.855	58.6	12.50	0.51
	porous B	4.500	4.475	88.7	0.00	0.50
	nonporous D	2.970	3.050	48.7	8.25	0.50
	nonporous E	1.825	2.985	71.8	20.50	0.50
1d	porous A (Kagomé)	6.435	6.365	60.3	13.25	0.50
	porous B	4.710	4.795	88.5	0.75	0.54
	nonporous D	2.970	3.190	52.0	8.25	0.50

[a] *EpiCalc* simulations analyze the lattice registry by rotating an overlayer lattice (b_1, b_2, and β) on a substrate lattice (a_1, a_2, and α) through a series of azimuthal angles (θ). In present study, following values are employed as the unit cell parameters of graphite substrate ($a_1 = a_2 = 0.246$ nm and $\alpha = 60°$). See the Supporting Information for details. [b] The V/V_0 value is a dimensionless potential for each azimuthal angle, which indicates the degree of commensurism between an overlayer and a substrate layer: $V/V_0 = 1$ for incommensurism, $V/V_0 = 0.5$ for point-online coincidence, and $V/V_0 = 0$ for commensurism on a nonhexagonal substrate.

system.[22] Note that for bisDBAs at the lowest concentration probed, 2.0×10^{-6} M, the number of molecules within a droplet (8 μL, 0.160 pmol) is not enough to cover a 1 cm^2 piece of graphite by (a combination of) porous motifs and obviously also not by nonporous motifs. At these submonolayer conditions, the porous motif is preferred. We have addressed the total molecular interaction energy (sum of intermolecular and molecule−substrate interactions at the level of a single molecule) via MM3 simulations (Table S4 of the Supporting Information).[42] In general, only a slight stabilization for molecules in a porous network is predicted at the individual molecule level, and it is questionable if the calculated differences between the different patterns have any predictive value also because solvation and solvent coadsorption effects are not taken into account. Especially, solvent coadsorption should play a role in the stabilization of the porous structures (vide infra). Furthermore, to analyze possible epitaxy between the overlayer and substrate, a lattice registry analysis was performed using EpiSearch subroutine in the *EpiCalc* program.[18,43] As a result, for all observed structures a number of fits classified as the point-on-line (POL) coincidence criteria were found within experimental error under certain search conditions (Table 2, also Supporting Information).[18] This implies that at least one POL coincidence exists in each molecular network, indicating that epitaxial stabilization plays a role in the monolayer formation. However, without thermodynamic information for the epitaxial effect, it is difficult to correlate it with the observed structural variations. At bisDBA concentrations exceeding those required for obtaining monolayer coverage, the close-packed nonporous networks become more favorable because the total enthalpy is decreased owing to the larger number of adsorbed molecules. The concentration dependency of the self-assembly of bisDBAs **1a**−**d** can therefore be understood as to arise from a balance between the different stabilities of the structures normalized to the single molecule level, including the stabilizing effect of solvent coadsorption, and the molecular density of the patterns.

2.5. Selection of Porous Networks. Another issue of interest is the selection of the porous networks. The differences in on the one hand the energies of intermolecular and molecule−substrate interactions and on the other hand the densities of the three porous networks A−C are small. On the basis of these grounds, it is difficult to understand the concentration-dependent appearance of the different porous patterns. As stated above, one can assume, however, that coadsorption of solvent molecules plays a crucial role. Indeed, sometimes bright features were observed in the hexagonal pore of the porous A structures and the rectangular pore of the porous B and C structures (e.g., the porous A structure in Figure S11 of the Supporting Information and the porous B structure in Figure 2).[44] Therefore, we modeled bisDBA network structures coadsorbed with TCB clusters via molecular mechanics simulations. In the simulation, TCB molecules are assumed to be connected via weak CH−Cl hydrogen bonds.[45,46] As can be seen in Figure 5, the hexagonal pores of the Kagomé structure of bisDBAs **1a** and **1d** as well as the rectangular pore of the porous B structure of bisDBA **1d** are occupied by TCB clusters. The same number of bright features as those experimentally observed fits nicely to the corresponding pores in the simulation, indicating that the observed bright spots can be ascribed to the specific number of coadsorbed TCB molecules. We believe that those images are actually snapshots revealing temporary ordered solvent clusters, which in general are dynamic in nature. Consequently, the selection of the porous networks is attributed, at least partially, to the coadsorption of solvent molecules that occupy the pores as clusters.[47] Interestingly, in other solvents than TCB (e.g., 1-phenyloctane or 1-octanoic acid), no Kagomé patterns are

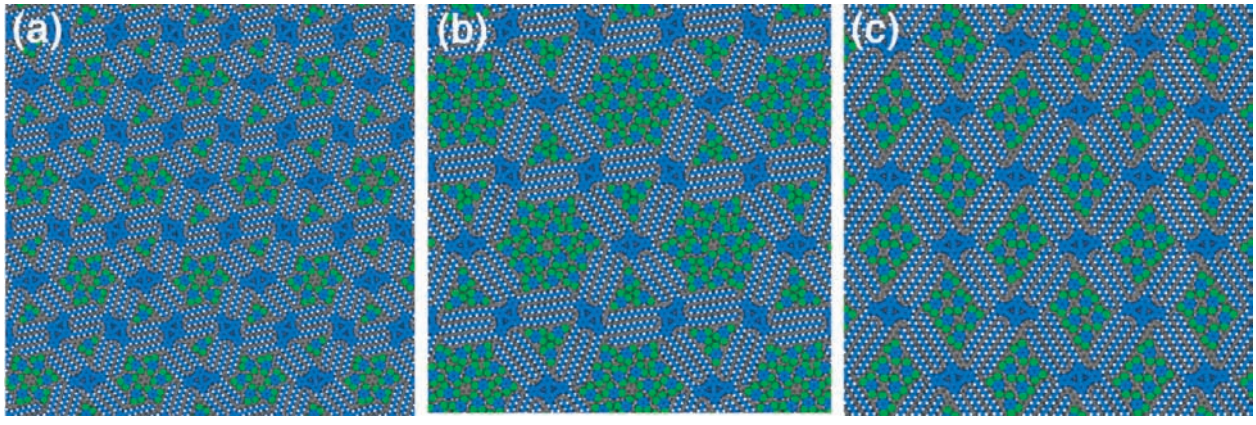

Figure 5. Models obtained via molecular mechanics simulations of the porous networks with coadsorbed TCB molecules for the Kagomé structure of **1a** (a), the Kagomé structure of **1d** (b), and the porous B structure of **1d** (c).

formed, regardless of the solute concentration, stressing the active participation of TCB in the monolayer formation.

Conclusions

We have accomplished STM measurements of a series of alkyl- and alkoxy-substituted rhombic-shaped bisDBA derivatives at the TCB/graphite interface. By changing the alkyl-chain length (i.e., tuning molecule−substrate and molecule−molecule interactions) and controlling the solute concentrations, bisDBAs were observed to form five structures, three porous structures (porous A, B, and C), and two nonporous structures (nonporous D and E). BisDBAs **1a** and **1b** with the shorter alkyl chains favorably form porous patterns, whereas bisDBAs **1c** and **1d** with the longer alkyl chains are prone to forming nonporous structures. However, upon diluting, the nonporous structures were observed to transform into porous structures. Under dilute conditions, partial formation of the Kagomé motif was observed for all compounds.

The main message of the present study is that concentration control is a powerful and general approach for structural selection, also in those cases where multiple pattterns coexist. Even more, variation in the alkyl-chain length is an extra option for structural selection. In addition, these prochiral molecules form both racemic compound and conglomerate phases, though no clear polymorph density dependency was observed, an intriguing issue in relation to the Wallach's rule in 3D crystals. The knowledge of how to select and favor the formation of specific patterns and in particular the porous templates will lead to the development of novel 2D host−guest chemistry, such as site-selective adsorption of two different components in size-controlled Kagomé lattices[31] or guest-induced switching between various porous structures.

Acknowledgment. This work is supported by a Grant-in-Aid for Scientific Research from the Ministry of Education, Culture, Sports, Science, and Technology, Japan, a Bilateral Program of Japan Society for the Promotion of Science, the Fund of Scientific Research - Flanders (FWO), K.U.Leuven (GOA), and the Belgian Federal Science Policy Office through IAP-6/27. J.A. thanks the Institute for the Promotion of Innovation by Science and Technology in Flanders (IWT).

Note Added after ASAP Publication. Two values in Table 2 and the citation in the last sentence of the Conclusions were incorrect in the version published ASAP November 6, 2009. The corrected version was published November 12, 2009.

Supporting Information Available: Synthetic procedures of **1a**−**d**, **2a**, and **2b**, experimental details (both STM measurements and molecular modeling), additional STM images, optimized structure of **1a**−**d**, **2a**, and **2b**. This material is available free of charge via the Internet at http://pubs.acs.org.

JA904481J

(44) A similar observation has been reported: See, ref 19f.
(45) (a) Taylor, R.; Kennard, O. *J. Am. Chem. Soc.* **1982**, *104*, 5063–5070. (b) Aakeröy, C. B.; Evans, T. A.; Seddon, K. R.; Pálinkó, I. *New. J. Chem.* **1999**, 145–152. (c) Abel, M.; Oison, V.; Koudia, M.; Maurel, C.; Katan, C.; Porte, L. *ChemPhysChem* **2006**, *7*, 82–85. (d) Oison, V.; Koudia, M.; Abel, M.; Porte, L. *Phys. Rev. B* **2007**, *75*, 03428.
(46) It has been well-known that chorine exhibits weak Cl−H hydrogen bonding (the distance ranges from 0.26 to 0.29 nm). Thus, we performed MP2/6-31g* optimization of a hexamer of TCB as the simplest case under vacuum. By comparison with six free TCB molecules, the sum of intermolecular interactions was estimated to be −2.48 kcal/mol. This indicates that by weak hydrogen bonding interactions TCB clusters are stabilized.
(47) Control experiments for bisDBA **1d** at the 1-phenyloctane/graphite interface at dilute conditions (1.5×10^{-6} M) or at dry conditions by the evaporation of TCB (1.3×10^{-6} M) resulted in the formation of the porous B and nonporous E structures or nonporous D structure, indicating the role of TCB coadsorption (also Figure S17 of the Supporting Information).